Mixing at Cross Junctions in Water Distribution Systems. II: Experimental Study

R. G. Austin[1]; B. van Bloemen Waanders[2]; S. McKenna[3]; and C. Y. Choi[4]

Abstract: The present experimental study focuses on the characterization of complex mixing phenomena at pipe intersections within pressurized water distribution networks. To examine the complete mixing assumption at a cross junction, a series of experiments were conducted in the turbulent regime ($R > 10{,}000$). The experimental setup consists of a cross junction with various sensors, pumps, and a data acquisition system to accurately measure solute concentration. Selected experimental results are compared to computational fluid dynamics (CFD) results. In addition, the water quality model associated with a standard water distribution network simulator (EPANET) was reevaluated based on CFD and experimental data. Corrections based on experimental results are incorporated into EPANET (AZRED 1.0) for use in a case study. The study concludes that the complete mixing assumption can potentially create considerable errors in water quality modeling. Further, severe errors are likely to occur in systems with many cross type junctions due to bifurcation of the incoming flows.

DOI: 10.1061/(ASCE)0733-9496(2008)134:3(295)

CE Database subject headings: Transport phenomena; Water quality; Water distribution systems; Potable water; Experimentation.

Introduction

Water quality models are widely used in analyses of water distribution systems. These network models have been used quite successfully for operational purposes, but in the context of providing real-time response for contamination events, the general mixing assumptions are most likely inadequate (van Bloemen Waanders et al. 2005; Romero-Gomez et al. 2006). Water security has been a concern of the water distribution community for several years, and it has become apparent that additional accuracy is critical to properly develop real-time response tools, especially if in situ sensor equipment will be used to help detect intrusions. Current models assume instantaneous and complete mixing at pipe junctions and several studies have contributed to growing evidence that this assumption may be inadequate. The "complete" mixing assumption becomes especially questionable at pipe cross junctions where there may be limited contact and retention time between the water flows in two incoming pipe legs. The impact of solute mixing at these intersections, geometric components of a network system, is the focus of this work.

[1]Graduate Research Assistant, Dept. of Agricultural and Biosystems Engineering, The Univ. of Arizona, Tucson, AZ 85721. E-mail: rgaustin@email.arizona.edu

[2]Research Scientist, Sandia National Laboratories, P.O. Box 5800, MS-0735, Albuquerque, NM 87185-0735. E-mail: bartv@sandia.gov

[3]Research Scientist, Sandia National Laboratories, P.O. Box 5800, MS-0735, Albuquerque, NM 87185-0735. E-mail: samcken@sandia.gov

[4]Professor, Agricultural and Biosystems Engineering, The Univ. of Arizona, Tucson, AZ 85721. E-mail: cchoi@arizona.edu

Note. Discussion open until October 1, 2008. Separate discussions must be submitted for individual papers. To extend the closing date by one month, a written request must be filed with the ASCE Managing Editor. The manuscript for this paper was submitted for review and possible publication on January 31, 2007; approved on June 15, 2007. This paper is part of the ***Journal of Water Resources Planning and Management***, Vol. 134, No. 3, May 1, 2008. ©ASCE, ISSN 0733-9496/2008/3-295–302/$25.00.

Studies examining two impinging jet streams with unconfined flows indicate that intersecting flows may bifurcate rather than mix (Ashgriz et al. 2001). Recent experimental and numerical results indicate that this bifurcation occurs in pipe junctions as well. In a study of a cross junction where all four flow rates were held equal (van Bloemen Waanders et al. 2005) approximately 87% of an NaCl tracer exited the junction in the outlet adjacent to the inlet where the tracer was introduced. Under the perfect mixing assumption, a 50% distribution would be expected. Both computational fluid dynamics (CFD) and experimental results were used in this study to describe transport phenomena at pipe cross intersections. However, the investigation was limited to the case of equal flow rates in each of the pipe legs.

Romero-Gomez et al. (2006) studied the same phenomena using a CFD model validated with experimental results to consider two additional flow scenarios through the cross joint (varying inflows with equal outflows and equal inflows with varying outflows). Additional experiments were performed to account for uncertainty with modeling parameters. The observations of the study suggested that the data necessary to improve water quality modeling software could be obtained by adjusting the turbulent Schmidt number, Sc_t, to match experimental data. The study addressed three selected scenarios at equal inflow and/or outflow rates. In their experimental study, the mismatch of the tracer mass flow rate averaged over 5%.

In this study, solute mixing at a cross junction with varying inflows and outflows is further evaluated both experimentally and numerically in order to account for the large range of operating conditions in water distribution systems. The experimental setup is largely based on the previous study reported by Romero-Gomez et al. (2006). However, the solute mass balance was greatly improved via a series of instrument calibrations and adjustments, i.e., the mismatch of the tracer mass flow rate is reduced to 2% or less in the present study. Experimental results are compared with those using CFD models from previous studies and perfect-mixing based EPANET models. It should be noted that Romero-Gomez et al. (2006) further focus on the computa-

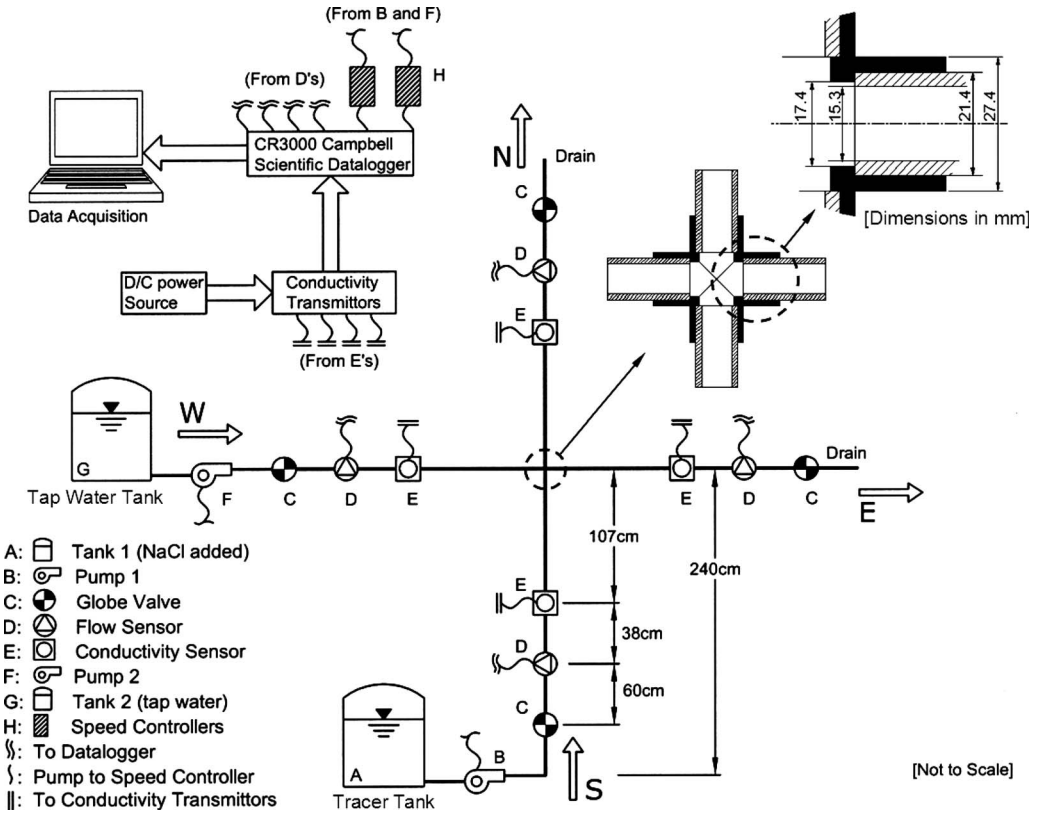

Fig. 1. A schematic of the experimental setup

tional (CFD) approach based on the present study. Finally, the impact on water quality modeling is illustrated by integrating the experimental results into EPANET for a multinode (exemplary) network [EPA (2002)].

Definitions and Scenarios

Sodium chloride (NaCl) is used as a soluble tracer throughout the experimental study. Two conventions are chosen to present the level of mixing in terms of the detected tracer: dimensionless concentration and the mass split. Dimensionless concentration is used to model concentrations at the outlets of pipe junctions to those of the inlets. This is also used to generalize the results such that they can be described independently of the background solute concentrations. The dimensionless concentration is described in the following:

$$C^* = \frac{C - C_W}{C_S - C_W} \tag{1}$$

where C^* is defined as the dimensionless concentration and C=concentration at the outlet of interest (east or north). C_S and C_W are the concentrations at the two inlets, south and west, respectively. Fig. 1 describes the experimental setup including two inlets from NaCl (south) and tap (west) water tanks.

Mixing is also described in terms of the mass of incoming NaCl exiting through either outlet. The mass split is not generalized for any set of incoming concentrations and depends on the incoming background NaCl concentrations. This measurement is useful as it directly describes where the species of interest is traveling and can therefore show where the introduced tracer travels. Mass split is described in the following:

$$\%\mathrm{NaCl}_{E\ or\ N} = 100 \times \frac{\dot{m}_{E\ or\ N}}{\dot{m}_E + \dot{m}_N} \tag{2}$$

where $\%\mathrm{NaCl}_E$ or $\%\mathrm{NaCl}_N$=percent mass split at either outlet; and $\dot{m}_{E\ or\ N}$=mass flow rate out the pipe leg of interest (east or north). $\dot{m}_S$ and $\dot{m}_N$=mass flow rates (kg/s) of the south and north pipe inlets, respectively.

In order to better understand the transport phenomena, three specific scenarios as well as generally varying flows are considered. Those scenarios and the general case were summarized in a companion paper by Romero-Gomez et al. (2008).

Romero-Gomez et al. (2008) suggested that the modeling variables could be greatly simplified to ratios of the inflows and outflows. This is preferable to the direct use of the Reynolds number at each pipe leg; thus, excessive data are not required to characterize the mixing at cross junctions for an infinite number of combinations of inlet and outlet flow rates. In the second scenario, for example, the Reynolds numbers at both outlets are equal whereas the Reynolds numbers at the inlets are different. The ratio of the inlet Reynolds numbers are defined as

$$\mathrm{R}_{S/W} = \frac{\mathrm{R}_S}{\mathrm{R}_W} \tag{3}$$

In the third scenario, the Reynolds numbers at both inlets are equal ($\mathrm{R}_{S/W}=1$), whereas the Reynolds numbers at the outlets are different. Thus, the ratio of the exit Reynolds numbers are defined as

$$\mathrm{R}_{E/N} = \frac{\mathrm{R}_E}{\mathrm{R}_N} \tag{4}$$

In the first scenario, therefore, $\mathrm{R}_{S/W}=1$ *and* $\mathrm{R}_{E/N}=1$. For the

general case, both the inlet and the outlet Reynolds ratios ($R_{S/W}$ and $R_{E/N}$) are varied. A matrix of data to be collected is constructed by varying the inflow and outflow ratios over the values 0.25, 0.65, 1.0, 1.5, 2.0, 3.0, and 4.0, for a total of 49 data sets to be collected. Each of these data sets is repeated three times, for a total of 147 experimental runs. Computational and experimental results by Romero-Gomez et al. (2006) showed that the mass split at a given $R_{S/W}$ and $R_{E/N}$ ratio combination for the cross junction remains nearly constant when $R > 10{,}000$. Thus, R_S, R_W, R_N, and R_E ranged from 10,000 to 42,000. For instance, R_S, R_W, R_N, and R_E are set at 26,151, 26,215, 25,807, and 25,601 (Scenario 1), respectively. For all 49 cases, flow rates were chosen such that (R_S+R_W) is equal to approximately 52,000 due to the physical characteristics and/or limitations of the experimental setup, sensors, and equipment. It should be noted that the majority of water distribution systems operate in the turbulent regime, and therefore the range of Reynolds numbers ($R > 10{,}000$) is justified in an attempt to reflect realistic operating conditions.

Experimental Setup and Preparation

The experiments were carried out in the Water Distribution Network Laboratory of the Water Village at the University of Arizona, Tucson, Ariz. The experimental setup consisted of a cross junction and piping system with various sensors, and a data acquisition system. The system included two pumps, two variable frequency controllers, a fresh water tank, a NaCl concentration tank, four gate valves, and a cross junction pipe system as shown in Fig. 1. Detailed dimensions of the cross junction (NIBCO Inc., Elkhart, IN) and PVC pipes were also presented. Each section of PVC pipe had a pair of flow and electrical conductivity sensors. A length greater than the equivalent of 65 pipe diameters (after the flow and conductivity meters) was used to allow for sufficient retention time so that turbulent flow could fully develop and thereby maximize mixing before entering the cross junction.

Concentration data (NaCl) and volumetric flow rates were collected at four locations (at each inlet and outlet of the cross junction) through conductivity sensors and flow meters. These readings were then used to calculate both the dimensionless concentration [Eq. (1)] as well as the mass split [Eq. (2)]. The flow rates were measured using paddle wheel sensors (FP-5600, the Omega Corporation, Stamford, Conn.). Electrical conductivity (to determine the concentration of NaCl) was performed using four-ring potentiometric probes and transmitters (CDE-1201, CDTX-1203, the Omega Corporation, Stamford, Conn.). The mass split was found by multiplying the concentration term by the flow rate at each of the pipe legs. Both of these numbers represent the amount of mixing at the cross junction and are presented in relation to the Reynolds number ratios, as defined in Eqs. (3) and (4) (see the section entitled "Results and Discussion"). The concentration of NaCl was calculated using a second-order polynomial curve relating conductivity to added salt.

A data logger (CR3000 model, Campbell Scientific, Logan, Utah) recorded sensor measurements to a computer in real time at a rate of one data point per second. These data were averaged over a 60 s interval to collect repeatable data by reducing the signal noise of the sensors. The flow sensor repeatability, as described by the manufacturer, is 0.5% of the full range or 0.36 L/min with a range of 1.34–71.9 L/min (0.3–19 gal./min). The flow rates in the experiments were maintained at or above 7.6 L/min (2 gal./min) and never approached 71.9 L/min (19 gal./min) to ensure that the sensors functioned properly. The flow sensors were calibrated by timing and collecting the discharge as water was pumped at a constant rate through the sensors. A total of 25 points were collected for each flow sensor at varying flow rates within the sensor's described range. The accuracy of the electrical conductivity sensors as described by the manufacturer is ±2% of the full sensor range (2 mS/cm). A two-point calibration was performed using commercially prepared calibration solutions.

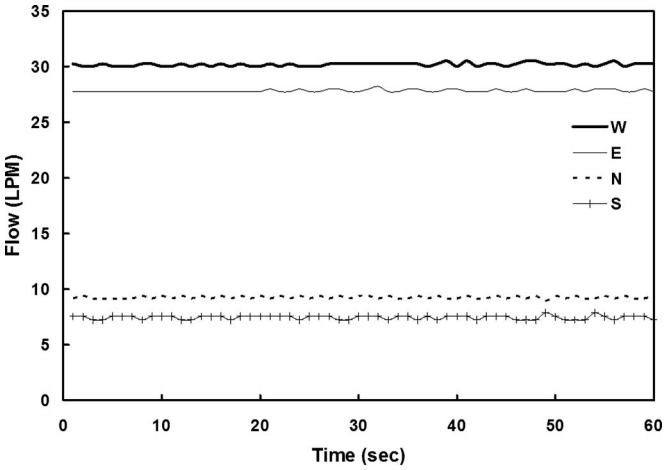

Fig. 2. An exemplary case of flow measurements: $R_{S/W}$ and $R_{E/N}=0.25$ and 3.0, respectively. LPM indicates liters per minute.

Results and Discussion

Observations of flow through the experimental system indicate that the flow behavior of the system appeared to be a steady state with no noticeable oscillations in flow or conductivity for all 49 cases of inflow and outflow combinations when $R > 10{,}000$. Figs. 2 and 3 illustrate flow rate and electrical conductivity readings collected for a typical run. Table 1 demonstrates a significant improvement over the previously reported results [an average of 5% mass balance error by Romero-Gomez et al. (2006)]. The decrease in the overall mass balance mismatch to an average of 1.9% is a result of a series of instrument calibrations and adjustments. The incoming concentration of NaCl at the west inlet was

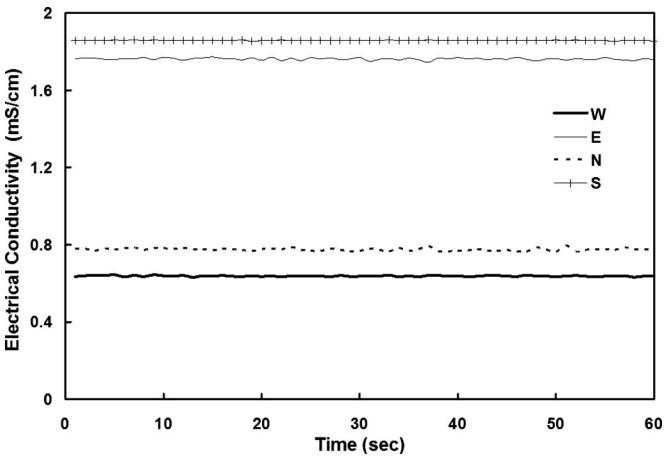

Fig. 3. An exemplary case of conductivity values when both $R_{S/W}$ and $R_{E/N}=1.0$ (Scenario 1)

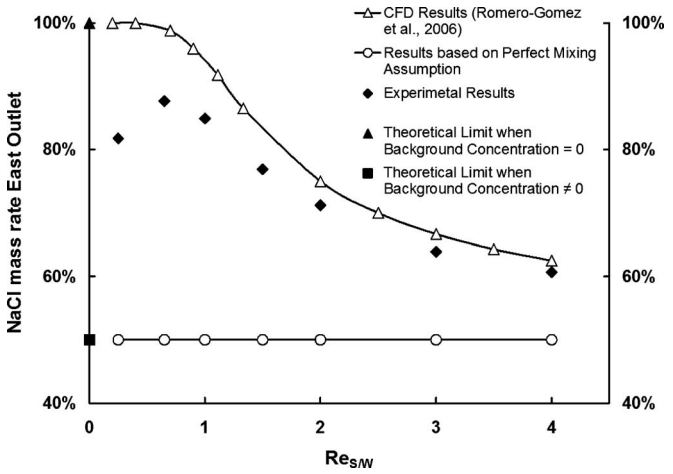

Fig. 4. NaCl mass rate splits from the experimental, numerical, and water quality model outcomes at different $R_{S/W}$ (east outlet), when $R_S \neq R_W$ and $R_E = R_N$ (Scenario 2)

intended to be kept constant; however, slight variations in the background conductivity of the tap water from run to run were observed as shown in Fig. 3. This background concentration does not affect the dimensionless concentration as the results are normalized. The presentation of the mass split results is, however, not independent of the incoming concentrations and will therefore be slightly affected. This is especially of interest in Scenario 2 as $R_{S/W} \rightarrow 0$ where the background concentration is important due to the small amount of the tracer entering the system.

Scenario 1: Equal Inflows and Outflows

For the case of equal inflows and outflows, three separate trials have been conducted with an equal flow rate at each of the four pipe legs. Perfect mixing for this scenario would give a dimensionless concentration of 0.5 and 0.5 and a mass split of 50 and 50%. For the present experiments, the Reynolds numbers at all legs are about 26,000 for Scenario 1. The average dimensionless concentration calculated from the experimental data is 91 and 11% through the east and north outlets, respectively. These numbers nearly add up to 100%, which indicates careful preparation of the experimental setup and calibration of both the flow and conductivity sensors to reduce experimental errors. With Reynolds numbers greater than 10,000, the C^* split remains nearly the same (approximately, $C_E^* = 90 \pm 3\%$). This C^* split appears in good agreement with previous experiments (van Bloemen Waanders et al. 2005). Scenario 1 is essentially a special case of Scenarios 2 and 3, and thus the experimental result by van Bloemen Waanders et al. (2006) is included in Figs. 5 and 7. The general trend for C^* at low R from laminar to turbulent flow will be of future research interest.

The mass split as calculated through Eq. (2) was 85 and 15% out the east and north outlets, respectively. If the incoming concentration at the west inlet were maintained perfectly at zero, the mass split and dimensionless concentration under this flow scenario should remain exactly the same. Both experimental and CFD model results demonstrate the dramatic difference from the assumption of perfect mixing.

Scenario 2: Equal Outflows, Varying Inflows

It should be noted that because the concentration and flow results at one outlet can be used to calculate values at the other outlet, only the results at the east outlet will be reported.

A discussion of R ratio limits (i.e., as $R_{S/W} \rightarrow \infty$, and $R_{S/W} \rightarrow 0$) of Scenario 2 follows to help clarify the results. As $R_{S/W} \rightarrow \infty$ the percent mass split will approach 50% because near instantaneous mixing should occur and an equal distribution will most likely result. As $R_{S/W} \rightarrow 0$ the mass split would become 100%, because as the flow decreases in the tracer inlet, less mixing occurs and the salt is eventually entirely diverted out the adjacent (east) outlet. This trend was reported by Romero-Gomez et al. (2006) and Romero-Gomez et al. (2008) using CFD results at the turbulent Schmidt number (Sc_t)=0.7 and presented in Fig. 4. This is not, however, the trend of the experimental data as plotted in the Fig. 4. With the experimental data the percentage of mass split reaches a maximum level around a Reynolds number ratio of 0.65. This trend is due to background NaCl concentrations above zero. With a background concentration, as $R_{S/W} \rightarrow 0$ there would be essentially no NaCl entering from the south inlet due to the reduced flow. All of the NaCl entering would come from the west inlet and would be due to background concentrations. The NaCl coming from the west inlet would then pass out of each outlet equally due to equal flow, giving a mass split of 50%. This trend is observed in the experimental data. In the water quality model, for example, a trace amount of chemical or biological agents introduced from the south inlet may be estimated either way. However, it is important to recognize that a trace amount of extremely toxic chemical contaminants or biological agents (e.g., a few anthrax spores) should be modeled with care; i.e., 100% of the introduced contaminant heads to the east outlet. With perfect mixing, 50% of the mass would flow out the east outlet for any $R_{S/W}$ ratio due to the outflows being equal.

Unlike the analysis based on %NaCl, background concentration (C_E^*) does not affect dimensionless concentration as it is defined to be normalized by the range of the inlet concentrations, as shown in Fig. 5. The trend of the dimensionless concentration is closer to that of the CFD results at Sc_t=0.7 presented by Romero-Gomez et al. (2006) and Romero-Gomez et al. (2008). As $R_{S/W} \rightarrow \infty$ it is expected that all of the flow will come from the south inlet containing the NaCl solution; the concentration of both of the outlets should asymptotically approach 1. As $R_{S/W} \rightarrow 0$ all of the entering water will be coming from the west inlet and the water leaving from the east outlet will approach the same concentration as the west inlet, resulting in a dimensionless concentration that asymptotically approaches 0. Both of these trends are observed in the experimental data. Similar trends are also observed with EPANET, although the differences in dimensionless concentration are significant.

Scenario 3: Equal Inflows, Varying Outflows

As the Reynolds number ratio of an outlet is increased, the tracer mass flow rate through that outlet will also increase. When $R_{E/N} \rightarrow \infty$ the mass split from the east outlet will approach 100% of the total mass flow rate because there will be no flow through the north outlet. As $R_{E/N} \rightarrow 0$, the situation is simply reversed with no flow in the east outlet. The mass rate split through the east outlet is therefore expected to be 0. These general trends can be observed in the data (see Fig. 6). Similar trends are observed using EPANET, although magnitudes are quite different for each $R_{E/N}$ case except in the limit as $R_{E/N} \rightarrow \infty$ and 0.

Table 1. List of Data for the Three Runs, including Reynolds Number Ratios of the Inlets and Outlets; Dimensionless Concentration at the East Outlet; Mass Split at the East Outlet; Percentage of Flow; and Mass Mismatch between the Incoming and Outgoing Flows

$R_{S/W}$	$R_{E/N}$	$\%NaCl_E$	C_E^*	Standard deviation C_E^*	% flow balance error	% mass balance error
0.25	0.25	51	0.59	1.1E−02	1.0	2.5
0.25	0.65	74	0.42	1.1E−02	1.3	4.0
0.25	1.01	82	0.35	8.8E−03	1.3	4.5
0.25	1.50	88	0.31	6.4E−03	1.4	4.0
0.25	2.00	91	0.28	5.8E−03	1.4	4.1
0.24	3.00	94	0.25	7.5E−03	1.5	4.1
0.25	3.95	96	0.24	5.2E−03	1.4	4.5
0.64	0.25	47	0.99	1.1E−02	1.5	2.5
0.65	0.65	79	0.85	6.2E−03	1.7	1.9
0.65	1.00	88	0.73	8.4E−03	1.6	2.4
0.65	1.51	91	0.63	5.1E−03	1.7	2.8
0.65	1.99	93	0.57	4.1E−03	1.8	3.0
0.64	3.03	95	0.51	6.3E−03	1.9	2.9
0.65	4.01	97	0.48	2.7E−03	2.0	3.7
1.00	0.25	39	1.01	6.8E−03	1.5	2.8
1.00	0.65	72	0.98	7.8E−03	1.8	0.9
1.00	0.99	85	0.91	5.2E−03	1.8	0.7
1.00	1.50	92	0.81	6.0E−03	1.8	1.4
1.00	2.00	94	0.74	7.6E−04	1.8	1.4
1.00	3.01	96	0.66	3.6E−03	1.9	1.8
1.00	4.02	97	0.62	3.1E−03	2.0	2.2
1.50	0.25	33	1.02	4.3E−03	1.7	2.7
1.50	0.65	62	1.00	1.2E−03	2.0	2.0
1.49	0.99	77	0.97	3.5E−03	1.9	0.7
1.50	1.50	88	0.92	7.1E−03	1.9	0.9
1.49	2.00	93	0.87	5.4E−03	2.0	1.1
1.49	3.01	96	0.79	8.5E−03	2.2	1.7
1.50	4.00	97	0.75	6.4E−03	2.1	2.0
2.00	0.25	30	1.01	6.0E−03	1.6	2.9
1.98	0.65	57	1.00	5.0E−04	1.6	2.2
1.99	1.01	71	0.99	2.7E−03	1.7	1.3
1.99	1.50	82	0.96	2.2E−03	1.8	0.5
2.00	2.00	88	0.93	3.7E−03	1.9	0.4
1.99	3.01	94	0.87	3.1E−03	1.9	0.4
1.98	3.96	96	0.83	4.8E−03	2.1	1.0
3.00	0.25	27	1.01	2.5E−03	1.6	2.1
2.99	0.65	51	1.00	3.0E−03	1.8	1.6
2.98	0.99	64	0.99	8.5E−04	1.7	1.3
2.99	1.51	76	0.98	3.7E−04	1.9	1.2
3.02	2.00	82	0.96	2.1E−03	1.8	0.8
3.01	2.96	89	0.93	2.7E−03	2.0	0.5
2.95	4.03	93	0.90	3.5E−03	1.9	0.3
4.04	0.25	25	1.02	1.7E−03	1.7	1.8
3.98	0.65	48	1.00	3.1E−03	1.8	1.6
3.97	1.00	61	0.99	4.1E−03	1.8	1.3
4.04	1.50	72	0.98	4.2E−03	1.9	1.1
3.97	2.01	79	0.97	8.2E−04	1.9	0.9
4.01	3.02	86	0.94	1.9E−03	2.0	0.8
4.02	4.03	90	0.93	2.0E−03	2.0	0.7

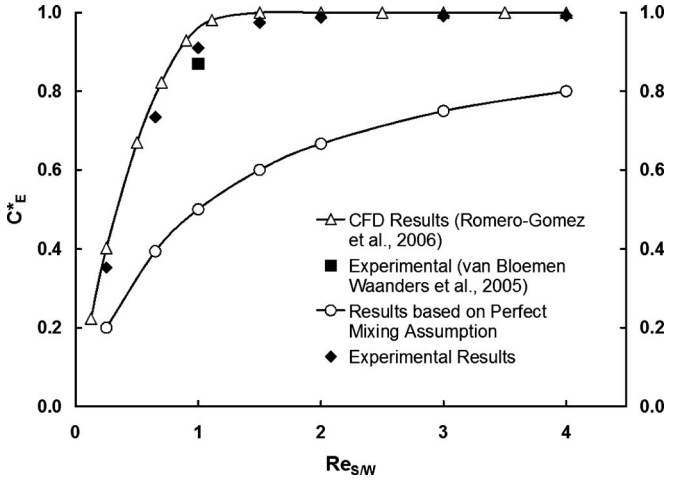

Fig. 5. Dimensionless concentrations from the experimental, numerical, and water quality model outcomes at different $R_{S/W}$ (east outlet), when $R_S \neq R_W$ and $R_E = R_N$ (Scenario 2)

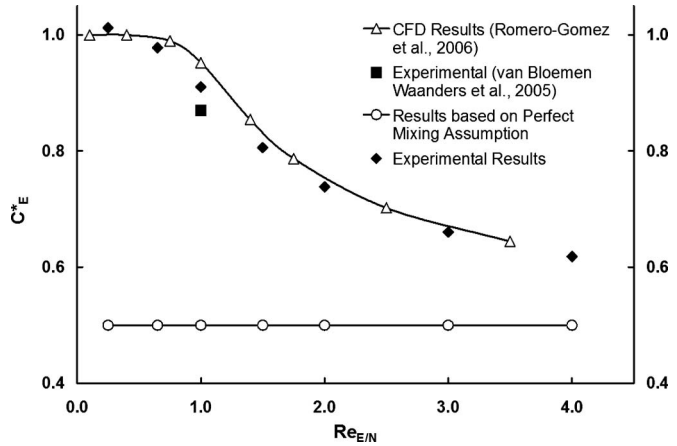

Fig. 7. Dimensionless concentrations from the experimental, numerical, and water quality model outcomes at different $R_{E/N}$ (east outlet), when $R_S = R_W$ and $R_E \neq R_N$ (Scenario 3)

In Fig. 7, the dimensionless concentration at the east outlet will become 0.5 as $R_{E/N} \rightarrow \infty$. This is because all of the water will exit through the east outlet, and half of the water coming from each inlet will be diluted. As $R_{E/N} \rightarrow 0$ it is expected that the infinitesimal amount of water flowing out of the east outlet will come from the south inlet. This will give a dimensionless concentration of 1. Both of the above-mentioned trends are in excellent agreement with the experimental data.

General Case: Varying Inflows and Outflows

All 49 of the desired data sets were repeated three times each for a total of 147 different data points. The average of each of the sets was used to construct the two-dimensional contour and three-dimensional graphs [Figs. 8(a and b)]. These figures present a general trend of the mixing ratios, including Scenarios 1–3. As the inlet ratio increases ($R_{S/W}$) so does the dimensionless concentration at the east outlet. As the outlet ratio ($R_{E/N}$) is increased, the dimensionless concentration also increases, though much less dramatically than in the direction of the inlet ratio. These plots provide information about the behavior of the cross junction

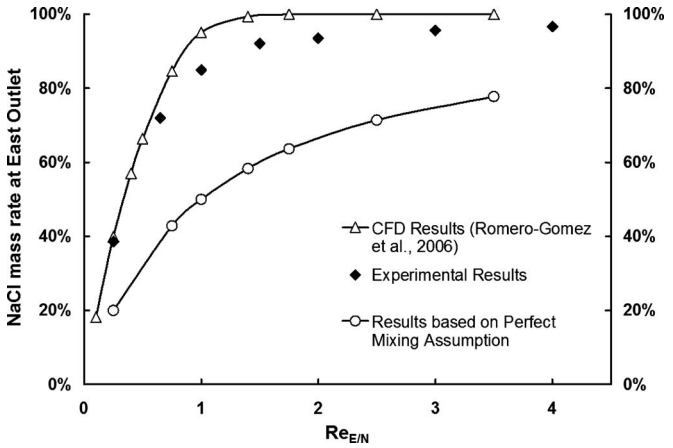

Fig. 6. NaCl mass rate splits from the experimental, numerical, and water quality model outcomes at different $R_{E/N}$ (east outlet), when $R_S = R_W$ and $R_E \neq R_N$ (Scenario 3)

transport phenomena over a useful range in real-world water distribution networks. The interpolated data can be integrated into the water quality model directly to obtain the dimensionless concentration over the R ratio ranges.

A Case Study: A Multinode (Exemplary) 4×5 Network

As an exemplary case, a 4×5 node pressurized piping network was introduced and the sensitivity of experimental results to predict water quality within a water distribution network was investigated. A grid shape with cross junctions was chosen because of its relevance to accurately forecasted contaminants at spatial scales in real-world municipal water systems. As shown in Fig. 9, water enters the system from the reservoir through the "intrusion point" and is removed through three demand points. Three demand points labeled *A*, *B*, and *C* each remove 379 L/min (100 gal./min) from the system. Injection of a solution of NaCl is simulated at the node labeled intrusion point at a rate of 3.79 L/min (1 gal./min) and a concentration of 100 mg/L for a mass flow of 378 mg/min. Each section of the pipe has a diameter of 30.5 cm (12 in.), a length of 152.4 m (500 ft), and a roughness of 100 for use in the Hazen–Williams equation. The entire model was created without a change in elevation. The corresponding Reynolds number in each pipe is also presented in Fig. 9.

The effect on transport for this configuration was examined using both current water quality modeling techniques (based on the assumption of complete mixing) as well as an updated model (using the results of the previously described experimental data). The hydraulic characteristics of the network were calculated by EPANET, and the water quality model produced results for the perfect mixing case. The same hydraulic conditions were used for the nonperfect mixing model. In each case where two adjacent inlets were encountered, the Reynolds number ratios [as described in Eqs. (3) and (4)] of each pipe were then calculated. This input was used to determine dimensionless concentration through linear interpolation of the experimental data set (see Table 1) rather than the perfect mixing assumption. This process was accomplished by changing the water quality at each of the pipe outlets (using C programming code, code name AZRED 1.0), forcing concentra-

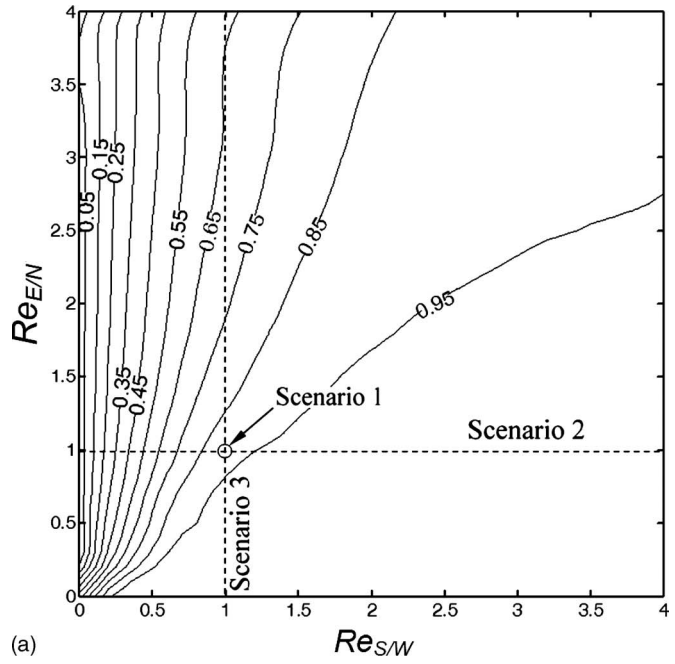

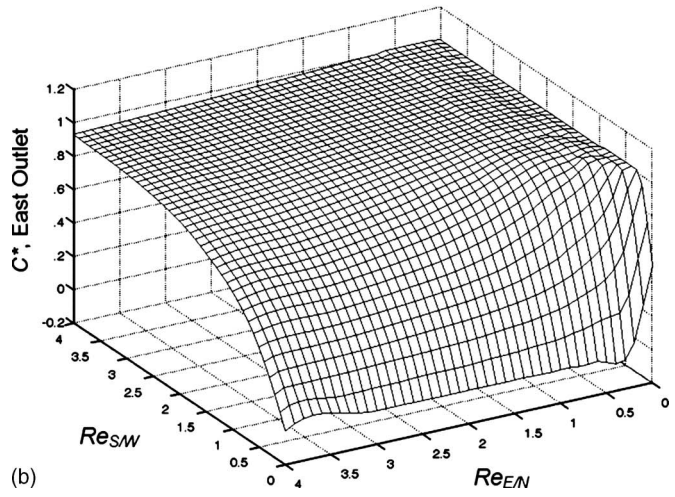

Fig. 8. Dimensionless concentration at the east outlet, average from three runs from 49 cases: (a) two-dimensional contours; (b) three-dimensional presentation

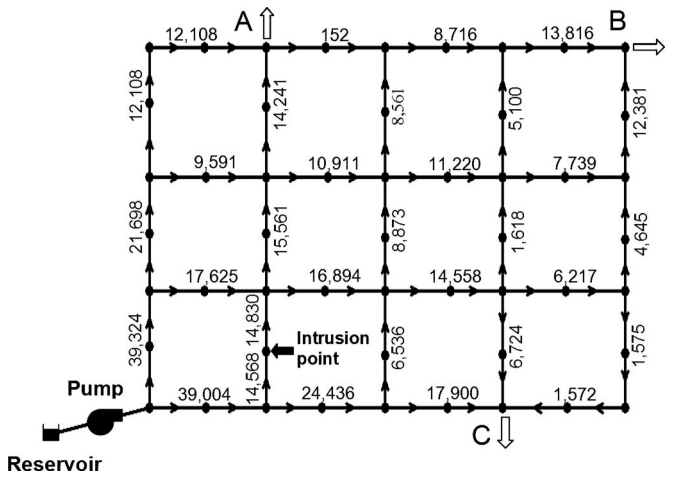

Fig. 9. Scenario building and corresponding EPANET setup for a 4×5 junction simplified water distribution network for an example case. The closed and open arrows represent the intrusion and demand points (*A* thru *C*), respectively. The Reynolds number is presented next to each pipe.

tion values to reflect the correct dimensionless concentration. Although the Reynolds numbers near the inlet are near 40,000 (fully turbulent zone), not all the pipes maintain $R > 10{,}000$. A further study is necessary to fully understand mixing phenomena at a cross junction for laminar and transitional flows. It is assumed that the experimental data set applies for all flow regimes, because all four legs at each cross junction maintain turbulent flows except one leg ($R = 1{,}618$).

Thus, the experimental cross-junction mixing results in this study show considerable deviation from the instantaneous mixing assumption and could have significant impact on chemical transport in large distribution networks. To assess this impact, we evaluated the effect of the mixing ratio plot on a multinode network. The water quality model in EPANET is modified based on the interpolation experimental data to determine an appropriate concentration depending on the hydraulic character of inlet and outlet points at each junction. A multinode network presented in Fig. 9 consists of five cross junction nodes with two incoming adjacent inlets. The remaining cross junction (i.e., the sixth junction located at the bottom right) had one incoming flow with three outgoing flows.

The results of the 4×5 network analysis indicate that there is a substantial difference between the water quality model based on the "perfect mixing" assumption and the one based on the "split mixing" results that reflect our experimental data. This difference can be seen through the concentration of NaCl at each of the demand points, as summarized in Table 2. The split mixing simulation indicates that the concentration at Demand Point *A* is much lower than the perfect mixing model suggests, i.e., 0.02 mg/L as compared to 0.27 mg/L. There are also significant differences in the concentrations at Demand Points *B* and *C*: 0.73 mg/L compared to 0.53 mg/L and 0.25 mg/L compared to 0.15 mg/L, respectively.

These differences are further illustrated through the use of contour lines based on the concentration of NaCl at each node in the system (see Fig. 10). For the case of the perfect mixing model, the salt concentration is much more uniform at locations downstream of the intrusion. This is in contrast to the split mixing model where the concentration is higher in the bottom right section of the system. This example demonstrates that water quality modeling may be modified based on the present experimental results, with significant improvement in networks containing cross junctions.

Table 2. NaCl Concentration (mg/L) and NaCl Mass Rate (mg/min) at Demand Points *A*, *B*, and *C* Using the Current and Modified Water Quality Models (Total Injected Salt = 378 mg/min)

	Assumption	*A*	*B*	*C*
NaCl concentration (mg/L)	Perfect mixing	0.27	0.53	0.15
	Split mixing	0.02	0.73	0.25
NaCl mass rate (mg/min)	Perfect mixing	102	200	56
	Split mixing	9	276	95

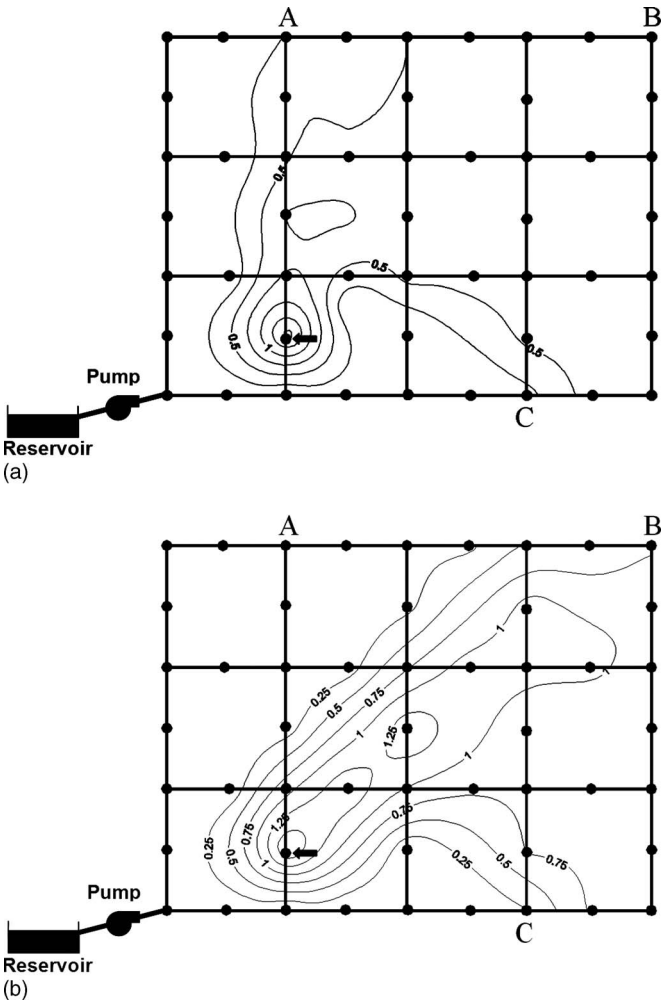

Fig. 10. Contours of NaCl concentration (mg/L); (a) based on perfect mixing assumption; (b) after modifications of the code. The arrow indicates the intrusion point, and concentration immediately after the dilution in the pipe is 1.77 mg/L.

Conclusion

This paper investigates the validity of the instantaneous mixing assumption at cross junctions and develops flow criteria to determine appropriate mixing rules. It shows that the complete mixing assumption can potentially create considerable errors in water quality modeling in particular with systems consisting of many cross junctions. This error is due to bifurcation of the incoming flows rather than perfect mixing. The data collected indicate that mixing at pipe cross junctions is in fact far from "perfect." The concentration of a species of interest at both outlets has been related to the incoming concentrations as well as to the ratios of the inlet and outlet flow rates. It is observed that small variations in the background concentrations have a significant impact on data taken under certain flow conditions (e.g., when there is little flow coming from the tracer source). The data collected are used to understand the significance of the perfect mixing assumption as well as a basis for the improved model itself.

A multinode case is investigated in which the intrusion of a contaminant is simulated. The EPANET code is altered to reflect experimental results by accounting for split mixing on a node-by-node basis. The comparison of the two indicates that the difference between the existing and modified water quality models is significant.

Acknowledgments

This work is supported by the Environmental Protection Agency/Department of Homeland Security (under Grant No. 613383D to the University of Arizona). Sandia is a multiprogram laboratory operated by Sandia Corporation, a Lockheed Martin Company for the United States Department of Energy's National Nuclear Security Administration under Contract No. DE-AC04-94AL85000. We would like to acknowledge additional graduate and undergraduate students at the University of Arizona, namely, Susan O'Shaughnessy, Jerry Shen, and Levi Johnson who have contributed their valuable time and efforts to the present work.

Notation

The following symbols are used in this paper:

C = NaCl concentration, kg L^{-1};
C^* = dimensionless concentration;
D = pipe diameter, m;
R = Reynolds number, $\rho DU/\mu$;
Sc_t = turbulent Schmidt number, $\mu_t/\rho D_t$;
U = average pipe flow velocity, m s^{-1};
μ = molecular viscosity, kg m^{-1} s^{-1};
μ_t = eddy viscosity, kg m^{-1} s^{-1}; and
ρ = mixture density, kg m^{-3}.

Subscripts

E = east outlet;
E/N = ratio of outlets, east to north;
N = north inlet;
S = south inlet;
S/W = ratio of inlets, south to west; and
W = west inlet.

References

Ashgriz, N., Brocklehurst, W., and Talley, D. (2001). "Mixing mechanisms in a pair of impinging jets." *J. Propul. Power*, 17(3), 736–749.

EPA. (2002). "EPANET 2.0." ⟨http://www.epa.gov/nrmrl/wswrd/epanet.html#Downloads⟩ (Jan. 10, 2007).

Romero-Gomez, P., Ho, C. K., and Choi, C. Y. (2008). "Mixing at cross junctions in water distribution systems. I: Numerical study." *J. Water Resour. Plann. Manage.*, 134(3), 285–294.

Romero-Gomez, P., Choi, C. Y., van Bloemen Waanders, B., and McKenna, S. A. (2006). "Transport phenomena at intersections of pressurized pipe systems." *Proc., 8th Annual Water Distribution System Analysis Symp.*, Cincinnati.

van Bloemen Waanders, B., Hammond, G., Shadid, J., Collis, S., and Murray, R. (2005). "A comparison of Navier-Stokes and network models to predict chemical transport in municipal water distribution systems." *Proc., World Water and Environmental Resources Congress*, Anchorage, Alaska.